이학석사학위논문

Suppressed upwelling events in the southwestern tropical Indian Ocean and the role of remote and local forcing

열대 남서인도양 용승 억제 현상 분석

2020년 8월

서울대학교 대학원
지구환경과학부
김 찬 미

Suppressed upwelling events in the southwestern tropical Indian Ocean and the role of remote and local forcing

지도 교수 나 한 나

이 논문을 이학석사 학위논문으로 제출함

2020년 8월

서울대학교 대학원
지구환경과학부
김 찬 미

김찬미의 이학석사 학위논문을 인준함

2020년 8월

위 원 장 남 성 현 (인)
부위원장 나 한 나 (인)
위 원 조 양 기 (인)

Abstract

Suppressed upwelling events in the southwestern tropical Indian Ocean and the role of remote and local forcing

Chanmi Kim

School of Earth and Environmental Sciences

The Graduate School

Seoul National University

The Seychelles-Chagos Thermocline Ridge (SCTR) in the southwestern tropical Indian Ocean is an upwelling region induced by negative wind stress curl between the southeast trades and equatorial westerlies. Previous studies have shown that the upwelling in the SCTR exhibits interannual variability associated with remote forcing from the eastern Indian Ocean. Easterly wind anomalies in the eastern Indian Ocean, which is related to the positive phase of El Niño-Southern Oscillation (ENSO) or the positive phase of Indian Ocean Dipole (IOD), produce downwelling Rossby waves that propagate westward and suppress the upwelling in the SCTR. The suppression can be stronger after both the ENSO and IOD exhibit positive phases. However, recent studies suggested that a role of local winds as well as the remote forcing cannot be neglected in the suppression of upwelling over the SCTR. In order to understand the relative contribution of the remote and local forcing, this study analyzes long-term reanalysis dataset over the tropical Indian Ocean during 1968–2017, identifies 9 suppressed upwelling events in the SCTR,

and investigates their characteristics focusing on the role of the remote forcing and the local winds. Both positive ENSO and positive IOD contributed to the suppression for 7 out of 9 suppression events during the 50 years, and composite analysis of the 7 events exhibit westward propagation of downwelling anomalies originated from the eastern Indian Ocean 3–6 months prior to the peak of suppression in the SCTR. However, only IOD showed positive phase before the 11-12 suppression event, and the downwelling anomalies from the eastern Indian Ocean and suppression of the upwelling in the SCTR were weaker than those of the 7 events. A strong suppression of the 78-79 event occurred without any significant influence of positive ENSO or positive IOD, but strong local winds in the SCTR played an important role on the extensive suppression of the upwelling over the southwestern tropical Indian Ocean. This study reveals that upwelling in the SCTR can be strongly suppressed not only by remote forcing but also by local winds, which would increase potential predictability of the upwelling variability in the SCTR.

Keyword: Tropical Indian Ocean, Upwelling, El Niño-Southern Oscillation, Indian Ocean Dipole, Seychelles-Chagos Thermocline Ridge

Student Number: 2018-22384

Table of Contents

List of Figures

1. Introduction

The Seychelles-Chagos Thermocline Ridge (SCTR) is an upwelling region in the southwestern Indian Ocean (Woodberry et al., 1989; McCreary et al., 1993). It has been also referred to as the Seychelles Dome or Thermocline Ridge of the Indian Ocean (Hermes and Reason, 2008; Yokoi et al., 2008; Jayakumar et al., 2011). Because of the nutrient-rich water caused by an upwelling, the SCTR is known to have high biological productivity (Xie et al., 2002; Dilmahamod et al., 2016). Also, the local warm sea surface temperature (SST) anomalies in the SCTR is associated with tropical cyclonic activity and anomalous rainfall in East Africa (Ummenhofer et al., 2009; Jury et al., 1999; Xie et al., 2002). The shallow thermocline depth caused by an upwelling, but high SST contribute to a strong air-sea interaction in the SCTR (Xie et al., 2002).

The upwelling is induced by negative wind stress curl between the southeasterly trades in the south and the equatorial westerlies to the north of the SCTR throughout the year, but relatively stronger in boreal winter (Xie et al., 2002; Hermes et al., 2008; Vialard et al., 2009) (Figure 1a). The southeasterly trades to the south of the SCTR drive South Equatorial Current with a weak near-surface southward flow whereas the equatorial westerlies to the north of the SCTR drive South Equatorial Countercurrent with a weak near-surface northward flow. The surface divergence associated with this is balanced by an upwelling which results the lifting of thermocline depth in the SCTR. In spite of the presence of the upwelling, the SST in the SCTR is above 27℃ almost all the time while those of other upwelling regions such as the eastern equatorial Pacific or Atlantic are below

25℃ due to the upwelling of the cold water (Vialard et al., 2009) (Figure 1b).

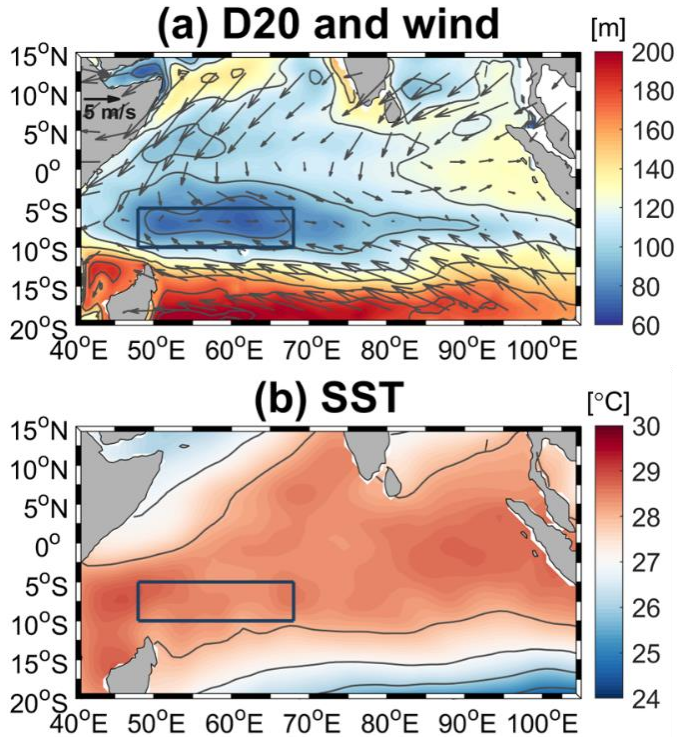

Figure 1. December climatology of (a) 20℃ isotherm depth (shading) and 10 m wind speed (vector) and (b) sea surface temperature over the tropical Indian Ocean during 1968–2017. The blue boxes indicate the Seychelles-Chagos Thermocline Ridge (5°S–10°S, 48°E–68°E).

The upwelling in the southwestern Indian Ocean exhibits interannual variability forced by remote wind from the eastern Indian Ocean. Particularly, the upwelling is suppressed in the SCTR associated with positive phase of El Niño Southern Oscillation (ENSO) or Indian Ocean Dipole (IOD) (Chambers et al.,

1999; Klein et al., 1999; Xie et al., 2002; Vinayachandran et al., 2002; Rao and Behera, 2005; Yu et al., 2005). The easterly wind anomalies in the eastern Indian Ocean induced by the positive ENSO or IOD drive westward propagation of downwelling Rossby waves, and thus the upwelling is suppressed in the SCTR (Masumoto and Meyers, 1998; Rao and Behera 2005; Yu et al., 2005). Moreover, in the co-occurrence years of the positive ENSO and IOD, the westward propagation of downwelling Rossby waves is sustained for a longer period due to the maintenance of easterly wind anomalies in the eastern Indian Ocean, which causes stronger suppression of the upwelling in the SCTR (Chakravorty et al., 2014).

Most of the previous studies have reported that the suppression of upwelling in the SCTR is related to remote forcing from the eastern Indian Ocean, which is related to the positive ENSO and IOD. In addition to the remote forcing, Tozuka et al. (2010] showed that the local wind forcing cannot be neglected in discussing the suppression of the upwelling in the SCTR. Using outputs from an Ocean Genenral Circulation Model, they conducted composite analysis for the period of 1980 to 2007. However, no detailed investigation of each suppression events was conducted focusing on the role of the remote and local forcing.

The present study analyzes long-term reanalysis dataset over the tropical Indian Ocean and identifies suppressed upwelling events in the SCTR during 1968-2017 considering strong interannual variability of the upwelling. Propagation characteristics of downwelling anomalies is investigated focusing on the role of remote forcing, and the role of local winds is also examined on the suppression

events. Rest of the paper is organized as follows. A description of the data sets and methodology used in this study is given in the next section. Sections 3 and 4 provide comparison between the suppressed upwelling events and discussions.

2. Data and Methods

The SST data were provided by Hadley Centre Global Sea Ice and Sea Surface Temperature (HadISST) with a spatial resolution of 1°, which uses reduced space optical interpolation applied to SSTs from the Marine Data Bank and ICOADS through 1981 and a blend of in-situ and adjusted satellite-derived SSTs for 1982-onwards (https://climatedataguide.ucar.edu/climatedata/sst-data-hadisst-v11). Subsurface temperature and sea surface height were obtained from the Simple Ocean Data Assimilation (SODA) product version 2.2.4 for the period 1968-2010 and version 3.4.2 for the period 2011-2017 (https://www2.atmos.umd.edu/~ocean/). The SODA is based on Parallel Ocean Program physics with a spatial resolution of 0.25° and 40 vertical levels for version 2.2.4 and 50 vertical levels for version 3.4.2. The upper 10-meter winds were from the National Center for Environmental Prediction-National Centers for Atmospheric Research (NCEP-NCAR) reanalysis data available on a T62 Gaussian grid. The Ocean Niño Index (ONI) provided by National Oceanic and Atmospheric Administration (NOAA) is used as an index of ENSO, which is computed as the SST anomalies averaged over the east-central equatorial Pacific Ocean, the Niño-3.4 region (5°S-5°N; 170°W-120°W). The Dipole Mode Index (DMI), the SST gradient between the western equatorial Indian Ocean (10°S-10°N; 50°E-70°E) and the south eastern equatorial Indian Ocean (10°S-0°N; 90°E-110°E), is also obtained from NOAA and used as an index of IOD. All the data is obtained as monthly means, and anomalies are calculated as deviations from their monthly climatology

during 1968–2017. Then, the monthly anomalies are low-pass filtered by 12-months to examine the interannual variability of the suppression of the upwelling in the SCTR.

The Seychelles Upwelling Index (SUI) is defined from area-averaged 20℃ isotherm depth (D20) of the target region (SCTR; 10°S-5°S, 48°E-68°E) for the period 1968-2017 in order to quantify the strength of upwelling (Figure 2a). A smaller SUI (shallower depth) indicates upwelling of the SCTR and a larger SUI (deeper depth) denotes suppression of the upwelling. A total of 9 events were identified as strong suppressed upwelling events based on the normalized SUI (out of one standard deviation). Figure 2b shows 7 events (72-73, 82-83, 94-95, 97-98, 02-03, 06-07, and 15-16) out of the 9 suppression events occurred after both the ENSO and IOD displayed strong positive phase. However, neither the ENSO nor IOD showed significant positive phase before the 78-79 suppression event, and only IOD showed positive phase before the 11-12 suppression event. Therefore, a composite analysis was conducted for the 7 events, and the results are compared with the other 2 events, 78-79 and 11-12.

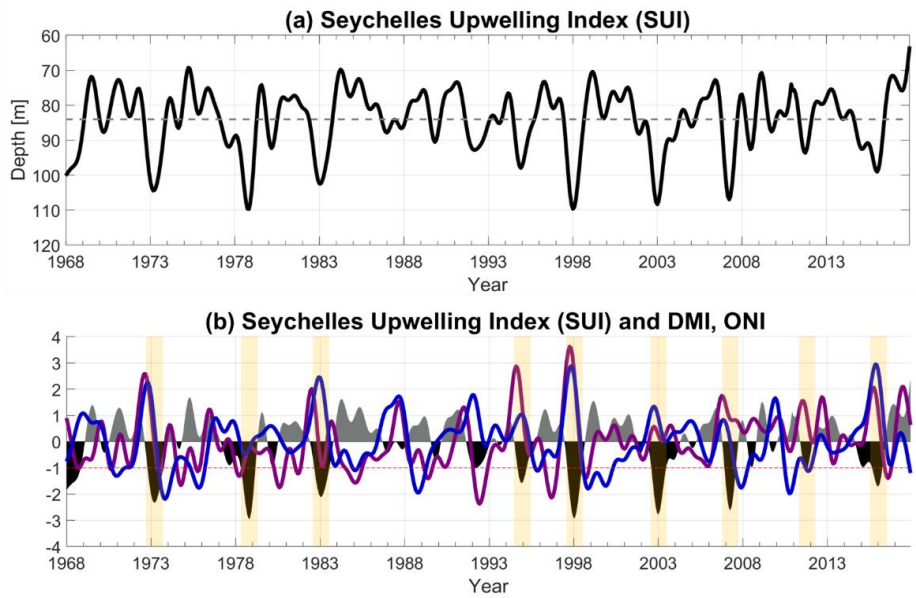

Figure 2. Time series of (a) Seychelles Upwelling Index (SUI) and (b) normalized time series of SUI (shaded black and gray), Dipole Mode Index (DMI; purple line), and Ocean Niño Index (ONI; blue line) for 1968–2017. The positive SUI means the upwelling in SCTR, and the negative SUI means the suppression of the upwelling in SCTR. The yellow shadings indicate the 9 suppressed upwelling events analyzed in this study.

3. Results

3.1. Composite of suppressed upwelling events

Figure 3 illustrates composites of D20 anomalies and winds stress anomalies for the 7 suppressed upwelling events during 1968-2017 (72-73, 78-79, 82-83, 94-95, 97-98, 02-03 and 06-07) extracted based on the SUI (Figure 2; yellow shaded). These 7 suppression events occurred after the ENSO and IOD displayed positive phase. Peak (0) indicates when the SUI exhibits negative maximum during the event, i.e. peak of the suppression, and the number between the bracket means the number of months prior to the peak or after the peak. Before the peak of the 7 suppression events, easterly wind anomalies were observed in the eastern Indian Ocean, which is related to the downwelling anomalies in the central equatorial Indian Ocean. Westward propagation of the downwelling anomalies in turn induced the suppression of upwelling in the SCTR after a few months. The downwelling anomalies emerged in Peak (-6) over 5°S-10°S in the central Indian Ocean and reached the eastern edge of SCTR in Peak (-4). The downwelling anomalies in the SCTR were maintained until Peak (+3) and started to disappear in Peak (+4). The downwelling anomalies started to appear over 5°S–10°S at first, however, the latitudinal extent expanded southward to 15°S in Peak (-2) and sustained for about four months. The composite results show that the strong easterly wind stress anomalies in the eastern Indian Ocean induce the downwelling anomalies, which propagate westward and strongly suppresse the upwelling in the SCTR. This result is consistent with the previous studies that showed the easterly

wind anomalies during positive ENSO and IOD generate downwelling anomalies which propagate westward and induce the suppression of upwelling in the SCTR (Xie et al., 2002; Vinayachandran et al., 2002; Rao and Behera, 2005; Yu et al., 2005).

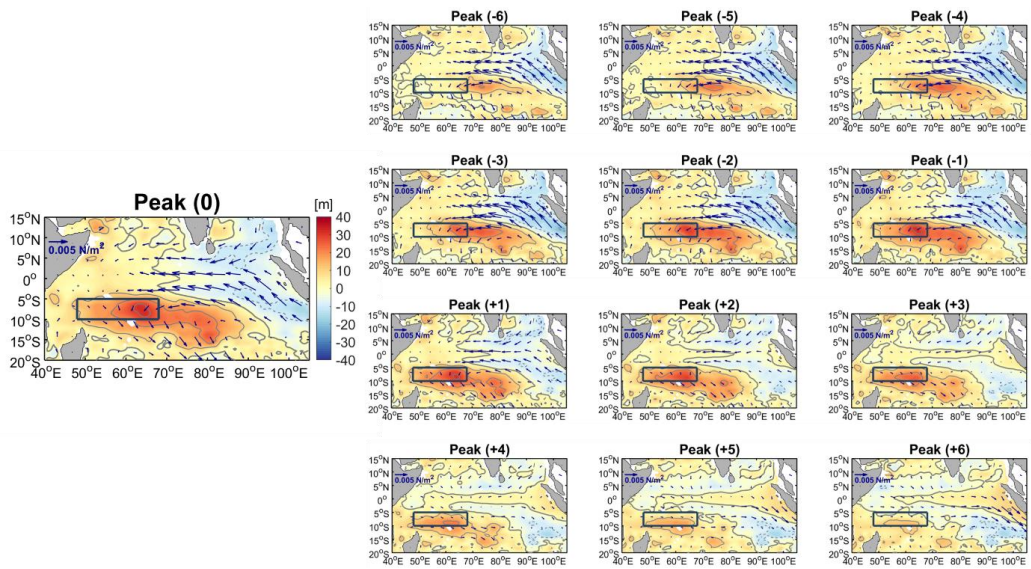

Figure 3. Composites of 20℃ isotherm depth anomalies and wind stress anomalies for the 7 suppressed upwelling events. Peak (0) means the peak month of the suppression of upwelling (deepest D20 anomalies) over the SCTR (blue box). Numbers between the bracket denote the number of months prior to the peak or after the peak.

The time-longitude plots of composite D20 anomalies for the 7 suppression events in Figure 4 present the characteristics of westward propagation for the SCTR (5°S–10°S, 48°E–68°E), to the east of SCTR (E-SCTR; 5°S–10°S, 68°E–88°E), to the south of SCTR (S-SCTR; 10°S–15°S, 48°E–68°E), and to the southeast of SCTR (ES-SCTR; 10°S–15°S, 48°E–68°E). Westward propagation of downwelling anomalies from the central Indian Ocean was observed both in the E-SCTR and ES-SCTR. The strong (> 20 m) positive D20 anomalies of the E-SCTR generated over 72°E–76°E after Peak (-5) and entered the SCTR in Peak (-4), which is consistent with Figure 3. The positive D20 anomalies of the ES-SCTR showed their maximum around 76°E–84°E, further east compared to those of E-SCTR, and they propagated toward the S-SCTR. It seems that the downwelling anomalies from the E-SCTR propagate further to the west than those from the ES-SCTR. The composite of 7 suppression events present that the propagation of downwelling anomalies from the central Indian Ocean is apparent throughout this events. Also, the downwelling characteristic at the peak of the 7 suppression events was consistent with that of the downwelling anomalies induced by the easterly wind anomalies in the eastern Indian Ocean during the positive ENSO and IOD (Figure 5a and 5b).

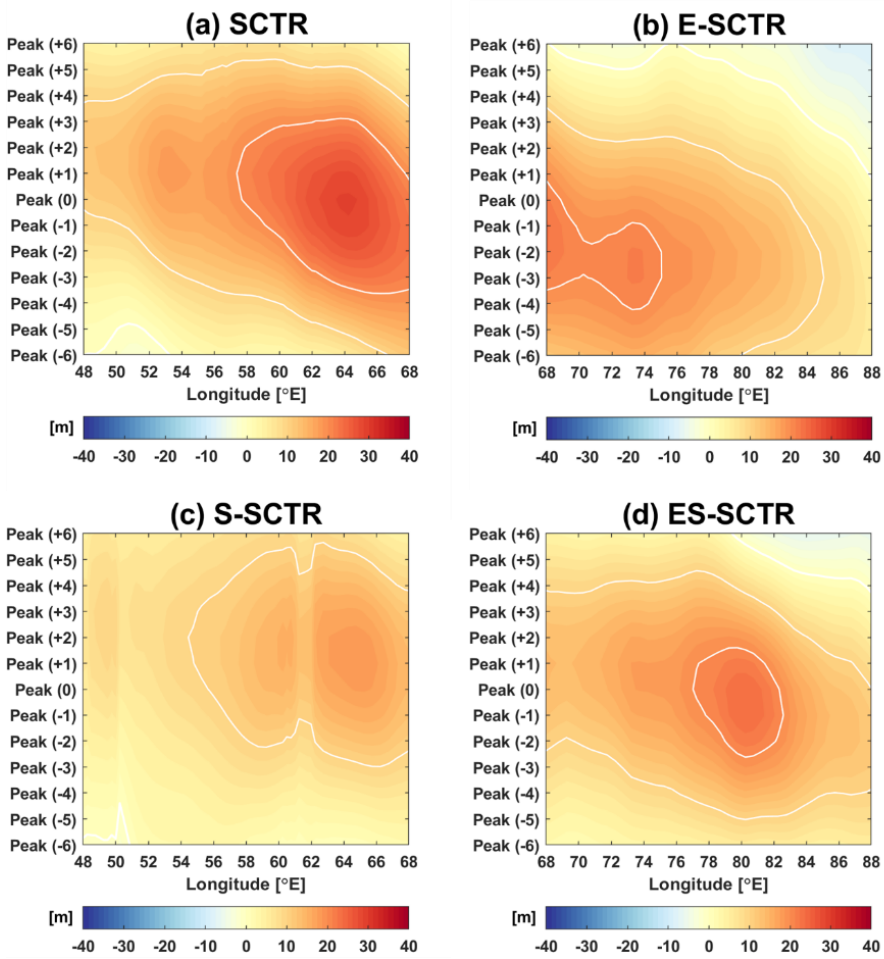

Figure 4. Time-longitude plots of D20 composites of the 7 suppressed upwelling events over (a) the SCTR (5°S–10°S, 48°E–68°E), (b) the eastern SCTR (E-SCTR; 5°S–10°S, 68°E–88°E), (c) the southern SCTR (S-SCTR; 10°S–15°S, 48°E–68°E) and (d) the southeastern SCTR (ES-SCTR; 10°S–15°S, 68°E–88°E). All of them were averaged over their latitude. White contours denote 10 m and 20 m contours.

Figure 5 shows composite D20 anomalies, wind stress wind anomalies, and zonal wind stress anomalies based on the ONI and DMI. The 36 months was identified as the co-occurrence months, 48 months as the positive ENSO, and 49 months as the positive IOD. Each spatial patterns indicate the peak of the positive ENSO and positive IOD. In the peak of the co-occurrence events, the easterly wind stress anomalies in the eastern Indian Ocean and the downwelling anomalies in the SCTR were stronger than the peak of the positive ENSO events and positive IOD events. Also, the co-occurrence events with ONI peak showed stronger easterly wind stress anomalies in the eastern Indian Ocean and stronger downwelling anomalies in the central Indian Ocean than the co-occurrence events with DMI peak. However, the spatial pattern when the ENSO showed positive phase showed the stronger easterly wind stress anomalies in the eastern Indian Ocean than the spatial pattern when only positive IOD occurred. Together with the strong remote forcing of easterly wind anomalies, the positive ENSO induced the stronger suppression of the upwelling in the SCTR than the positive IOD. The spatial pattern of the co-occurrence events was similar with the results of composite of 7 suppression events which show the strong easterly wind anomalies in the eastern Indian Ocean and downwelling anomalies in the SCTR.

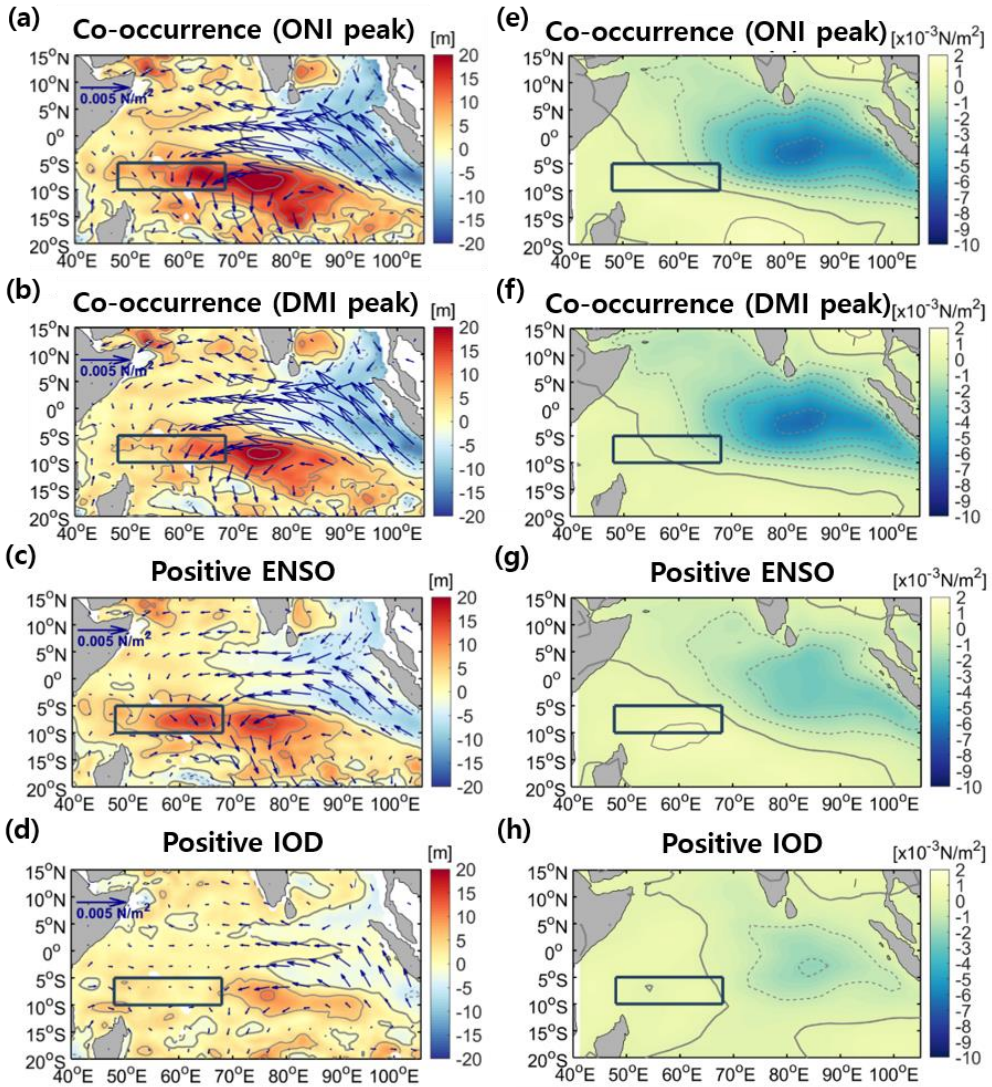

Figure 5. Composite anomalies of (a-d) D20 (shading) and wind stress (vector), and (e-h) zonal wind stress based on the ENSO index (ONI) and the IOD index (DMI). (a,e) and (b,f) display those for the co-occurrence months of the positive ENSO and positive IOD when the positive ONI and DMI exhibit their peaks, respectively. (c,g) display the composite anomalies for the positive ENSO, and (d,h) display those for the positive IOD.

3.2. 78-79 event

The spatial patterns of D20 anomalies and wind stress anomalies during 78-79 suppressed upwelling event is shown in Figure 6. During this event, A strong suppression of the upwelling occurred without any significant influence of poisitive ENSO or IOD. The downwelling anomalies were developed over the east of SCTR in Peak (-6), extended to the south and southeast of SCTR, and were maintained even after the peak of the suppression. The propagation of downwelling anomalies from the central Indian Ocean between 5°S-10°S were absent during this event, however, the downwelling anomalies between 10°S-15°S, 80°E-90°E in Peak (-6) propagated to the west and suppressed the upwelling to the south of the SCTR. Also, the downwelling anomalies over 5°S-10°S only stayed in SCTR rather than propagating from the central Indian Ocean, and the strong downwelling anomalies south to the SCTR were found during this period. The propagation of the downwelling anomalies from southeast Indian Ocean which suppressed the upwelling of southwest Indian Ocean was not consistent with the propagation characteristic of downwelling anomalies induced by remote forcing during positive ENSO and IOD. The propagation characteristic of this event is that the location of the downwelling anomalies was expanded further south compared to the downwelling anomalies of the 7 suppression events. On the other hand, the southerly or southeasterly wind stress anomalies were found in the eastern Indian Ocean instead of the easterly wind stress anomalies which is known as the remote forcing of the suppression in the SCTR during the positive ENSO and IOD. This means that the remote forcing which is normally induced by the easterly wind

anomalies in the eastern Indian Ocean was weaker than the other suppression events in this event. Thus, other impact, such as local winds forcing, might induce the strong suppression of the upwelling in the SCTR rather than the remote forcing. Also, unlike the composite D20 anomalies of 7 suppressed upwelling events, the opposite phase of D20 anomalies in the western and eastern Indian Ocean were found south to the equator.

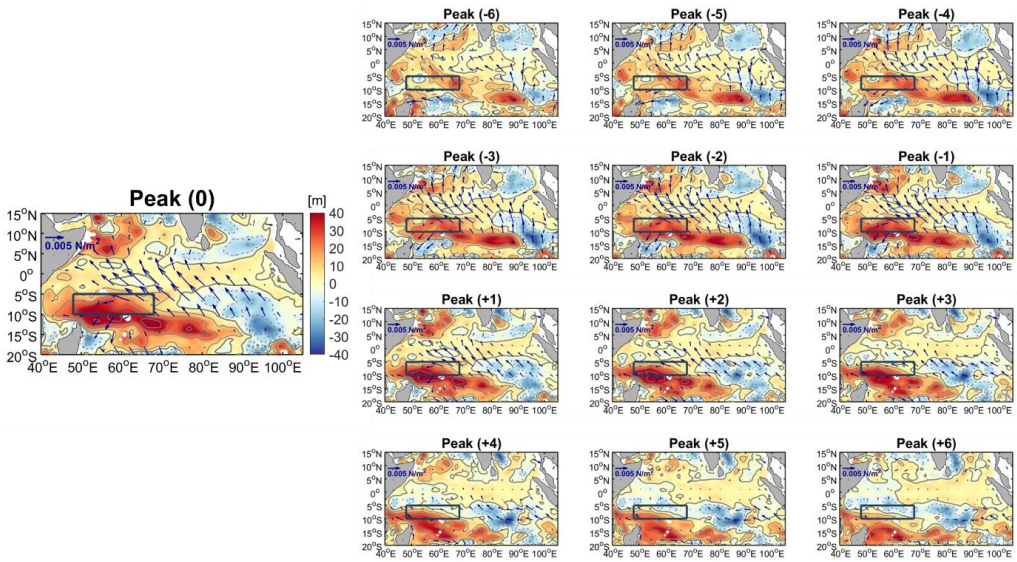

Figure 6. Spatial patterns of D20 anomalies and wind stress anomalies for the 78-79 event. Peak (0) means the peak month of the suppression of upwelling (deepest D20 anomalies) over the SCTR (blue box). Numbers between the bracket denote the number of months prior to the peak or after the peak.

The time-longitude plots of D20 anomalies for 78-79 event averaged over latitude over SCTR, E-SCTR, S-SCTR, and ES-SCTR are shown in Figure 7. The strong downwelling anomalies appeared in the SCTR (> 20 m), however, there was no propagation of downwelling anomalies from E-SCTR unlike the propagation of downwelling anomalies in the 7 suppression events. The strong (> 30 m) downwelling anomalies starting at 64°E inside the SCTR in Peak (-3) started to propagate to the west of SCTR until Peak (-3). In ES-SCTR, the strong (> 20 m) downwelling anomalies over 83°E-88°E in Peak (-6) propagated westward further to the west of S-SCTR. This propagation characteristic of downwelling anomalies is not consistent with that of 7 suppression events which is caused by the remote forcing induced by the easterly wind anomalies during the positive ENSO and IOD. This implies that the strong downwelling anomalies to the south and southeast of the SCTR are induced by the other factor, such as local winds, rather than the remote forcing. On the other hand, the upwelling anomalies in 88°E started to propagate westward to the east of SCTR until Peak (+6).

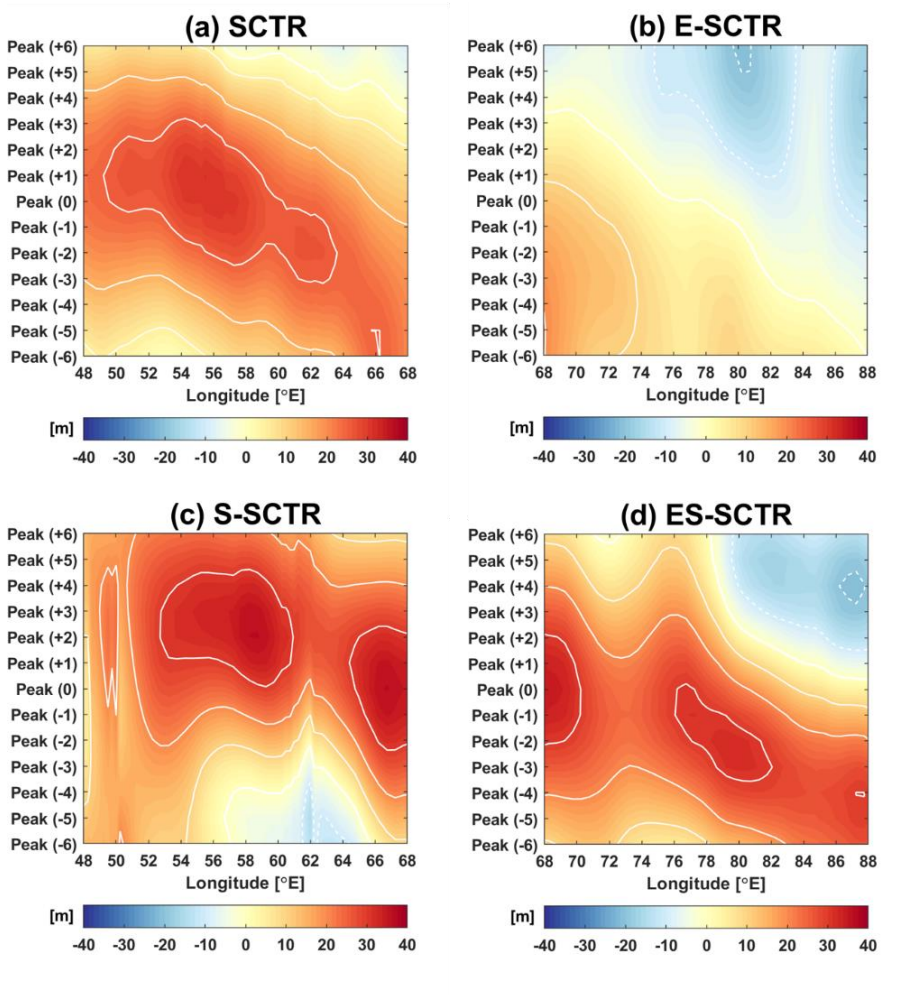

Figure 7. Time-longitude plots of D20 anomalies of the 78-79 event over (a) the SCTR (5°S–10°S, 48°E–68°E), (b) the eastern SCTR (E-SCTR; 5°S–10°S, 68°E–88°E), (c) the southern SCTR (S-SCTR; 10°S–15°S, 48°E–68°E) and (d) the southeastern SCTR (ES-SCTR; 10°S–15°S, 68°E–88°E). All of them were averaged over their latitudes. White contours denote 0 m, 10 m, 20 m, and 30 m contours.

3.3. 11-12 event

Figure 8 shows the spatial patterns of D20 anomalies and wind stress anomalies during 11-12 event. The suppression of the upwelling occurred after only IOD displayed positive phase in this event. The downwelling anomalies in western part of SCTR, 70°E-80°E and 90°E-100°E, were found in Peak (-6). The downwelling anomalies in 70°E-80°E and 90°E-100°E started to merge in Peak (-2) and propagated westward to the SCTR. The propagation of downwelling anomalies only existed north to the 10°S which is known as a feature of westward propagation of downwelling Rossby waves during the positive IOD (Rao and Behera, 2005; Yu et al., 2005). Also, the propagation of downwelling anomalies from the central Indian Ocean was weaker than the propagation of downwelling anomalies during 7 suppression events. The easterly wind stress anomalies in the eastern Indian Ocean were absent during this event, instead the southerly or southeasterly wind stress anomalies similar with that of the 78-79 event were shown in the eastern Indian Ocean. However, regardless of the lack of easterly wind anomalies in the eastern Indian Ocean, the weak westward propagation of downwelling anomalies was occurred, and it is considered as the effect of the remote forcing during the positive IOD. This indicates that the downwelling anomalies induced by the remote forcing during the positive IOD contributes to the suppression of the upwelling in the SCTR, but are less significant than the remote forcing induced by easterly wind anomalies in the eastern Indian Ocean during 7 suppression events.

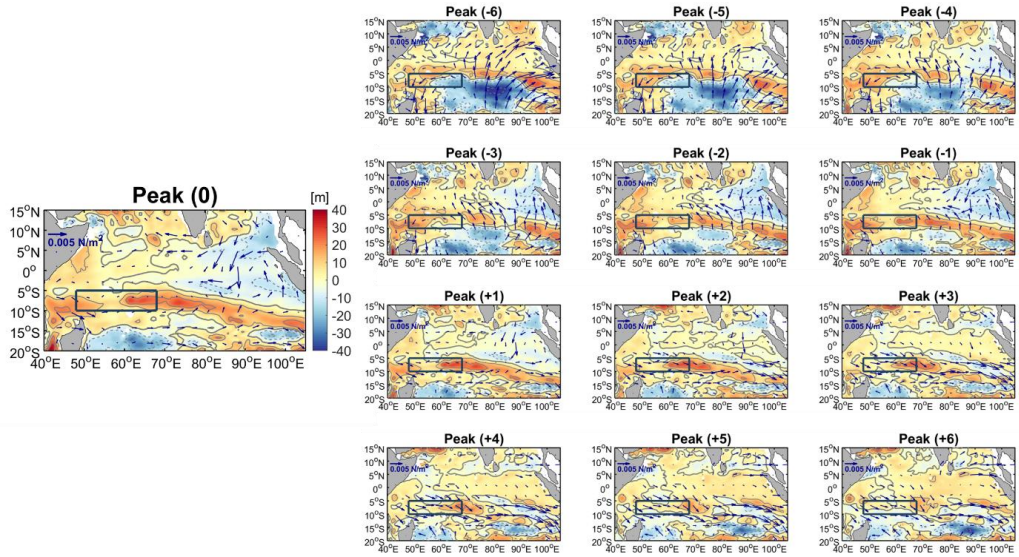

Figure 8. Spatial patterns of D20 anomalies and wind stress anomalies for the 11-12 event. Peak (0) means the peak month of the suppression of upwelling (deepest D20 anomalies) over the SCTR (blue box). Numbers between the bracket denote the number of months prior to the peak or after the peak.

The time longitude plots of D20 anomalies for 11-12 event in Figure 9 show the characteristics of westward propagation for the SCTR, E-SCTR, S-SCTR, and ES-SCTR. During this event, weaker westward propagation of downwelling anomalies (< 20 m) from the central Indian Ocean compared to that for 7 suppression events was observed the E-SCTR. The weak downwelling anomalies, smaller than 10 m, were found over S-SCTR and ES-SCTR. The downwelling anomalies, greater than 10 m, were found in the west of SCTR in Peak (-6), and

also found in the center of E-SCTR in Peak (-3). The downwelling anomalies (> 10 m) in E-SCTR then propagated westward to the west of SCTR, spreading shorter distance than the 7 suppression events. This propagation of downwelling anomalies was weaker, and had smaller magnitude than the propagation of downwelling anomalies during 7 suppression events, and only found in the north to the 10°S. The positive IOD during this event is considered as a factor of generating the weak propagation of downwelling anomalies from the E-SCTR and suppressing the upwelling in the SCTR.

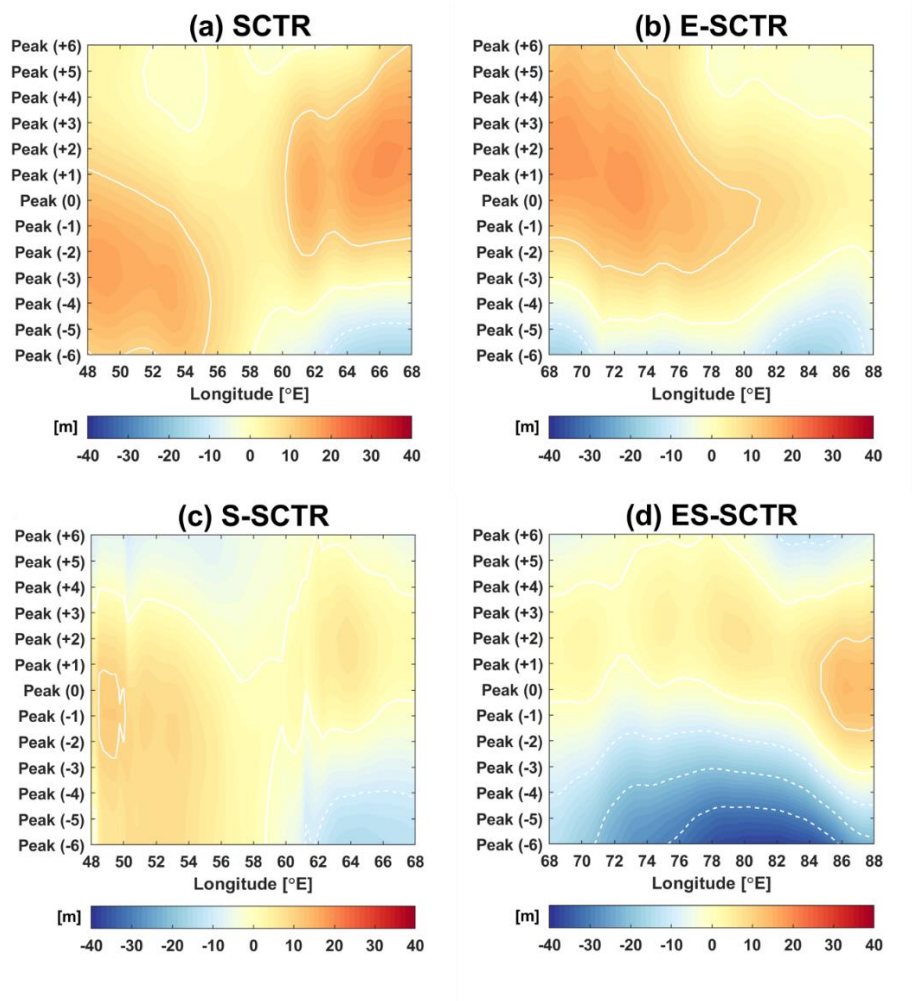

Figure 9. Time-longitude plots of D20 anomalies of the 11-12 event over (a) the SCTR (5°S–10°S, 48°E–68°E), (b) the eastern SCTR (E-SCTR; 5°S–10°S, 68°E–88°E), (c) the southern SCTR (S-SCTR; 10°S–15°S, 48°E–68°E) and (d) the southeastern SCTR (ES-SCTR; 10°S–15°S, 68°E–88°E). All of them were averaged over their latitudes. White contours denote 0 m and 10 m contours.

3.4. Role of local winds in the SCTR

The spatial patterns of wind stress curl anomalies at the peak of each suppression events and the time series of area-averaged mean of wind stress curl anomalies in the SCTR are shown in Figure 10 to investigate the role of local winds on the suppression of the upwelling in the SCTR. The positive phase of wind stress curl anomalies means the suppression favorable winds in the SCTR. During the peak of suppressed upwelling events, the positive winds stress curl anomalies were shown in the SCTR except 11-12 event. Especially, strong wind stress curl anomalies were found in the SCTR in the south and southeast of the SCTR during the peak of 78-79 event. The positive wind stress curl anomalies in the SCTR during 78-79 event were strongest 2 months before the peak of the suppression, and were maintained until the peak of the suppression in the SCTR. Therefore, the strong suppression of the upwelling in the SCTR and south and southeast of the SCTR during 78-79 event are contributed by the strong wind stress curl anomalies over the SCTR and south and southeast of the SCTR. However, the weak negative wind stress curl anomalies were shown in the SCTR during the peak of 11-12 event, but the strong positive wind stress curl anomalies were found 5 months before the peak of the suppression in the SCTR. The strong positive wind stress curl anomalies 5 months before the peak of the suppression in this event also contribute to the suppression of the upwelling in the SCTR together with the remote forcing induced by the positive IOD. During the 7 suppression events, the wind stress curl anomalies in the SCTR displayed weak positive phase, the suppression favorable winds. Also, the local wind stress curl anomalies in the SCTR were weak

throughout 6 months from the peak of the suppression to 6 months after the peak of the suppression in the SCTR. This indicates that the local winds in the SCTR during the 7 suppression events played a less important role on the suppression of the upwelling compared to the remote forcing induced by the positive ENSO and positive IOD.

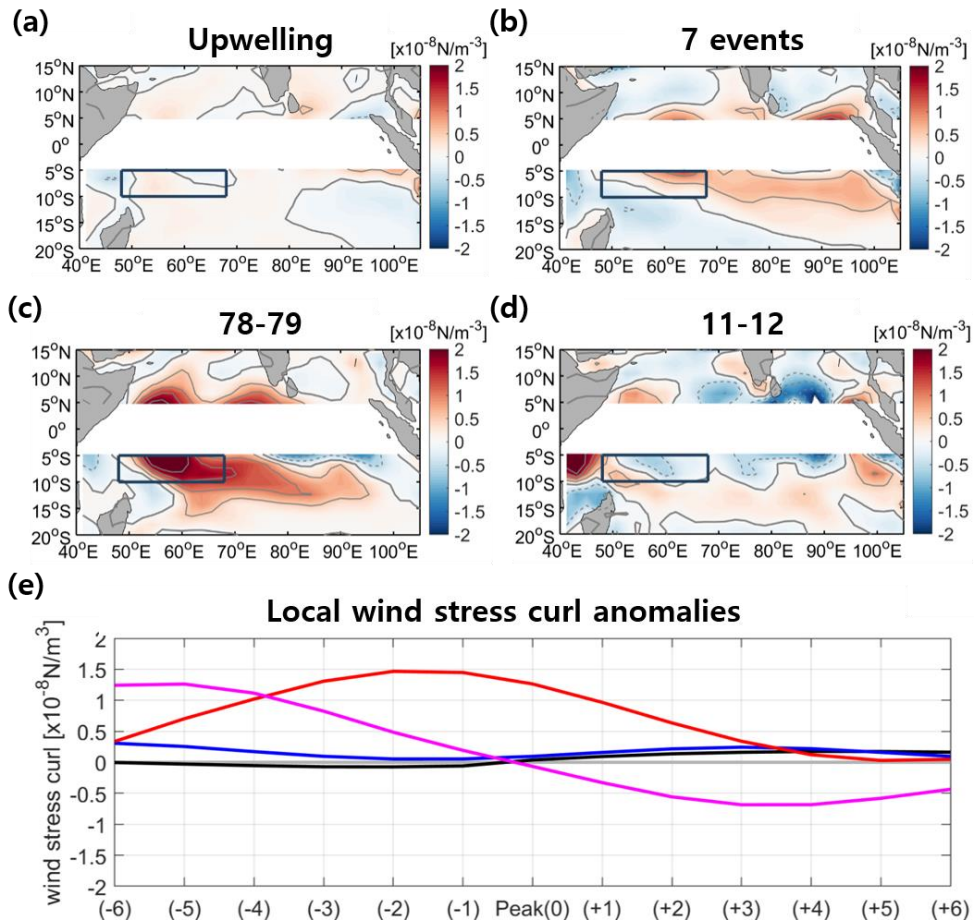

Figure 10. (a-d) Spatial patterns of wind stress curl anomalies at the peaks, and (e) time series of local wind stress curl anomalies (averaged over the blue box, the SCTR) for 6 months prior to and after the peaks each. The peaks are for the composites of upwelling (a, black in e), the composites of 7 suppression events (b, blue in e), 78-79 event (c, red in e), and 11-12 event (d, magenta in e).

4. Discussion and Conclusion

This study investigated the suppressed upwelling events in the SCTR focusing on the role of the remote forcing and the local winds. The suppression events were classified into three categories, the 7 suppression events occurred after both the ENSO and IOD displayed positive phases, the 78-79 event occurred without any significant positive ENSO nor positive IOD, and the 11-12 event occurred after only IOD showed significant positive phase. The propagation characteristics of the 7 suppression events showed the typical westward propagation of downwelling anomalies which is induced by the easterly wind anomalies in the eastern Indian Ocean during the positive ENSO and positive IOD. During the 78-79 event, the propagation of downwelling anomalies was very weak compared to those of the 7 suppression events. Rather, strong local winds contributed to the strong suppression of the upwelling over the SCTR and to the south and southeast of the SCTR. During the 11-12 event, the weak propagation of downwelling anomalies was induced after the IOD displayed positive phase, and the strong local winds played a significant role on the suppression of the upwelling in the SCTR starting about 5 months prior to the peak of the suppression.

The 78-79 event and the 11-12 event show that local winds in the SCTR can contribute to the strong suppression of the upwelling, though remote forcing is known as a main reason for the suppression from previous studies. However, a quantitative comparison between the contribution of the remote forcing and the local winds is remained as a future study. It will clarify the relative role of the

remote forcing and the local winds on the suppression of the upwelling in the SCTR. In addition, the suppression-favorable local winds need to be further examined, particularly what makes the suppression-favorable winds in the SCTR is still in question. From the result of composite analysis based on the ONI and DMI, it is revealed that the strong easterly wind stress anomalies in the eastern Indian Ocean are extended to the west, close to the SCTR (Figure 5). The expansion of the easterly wind stress anomalies during the positive ENSO and IOD can possibly affect the local winds in the SCTR. Therefore, the source of remote forcing, i.e. ENSO and IOD, might also influence the formation of the suppression-favorable local winds in the SCTR. Despite the above limitations, this study would contribute to a better understanding of the interannual variability of the upwelling in the SCTR and a possible prediction of the upwelling by emphasizing the role of local winds together with the effects of the ENSO and IOD.

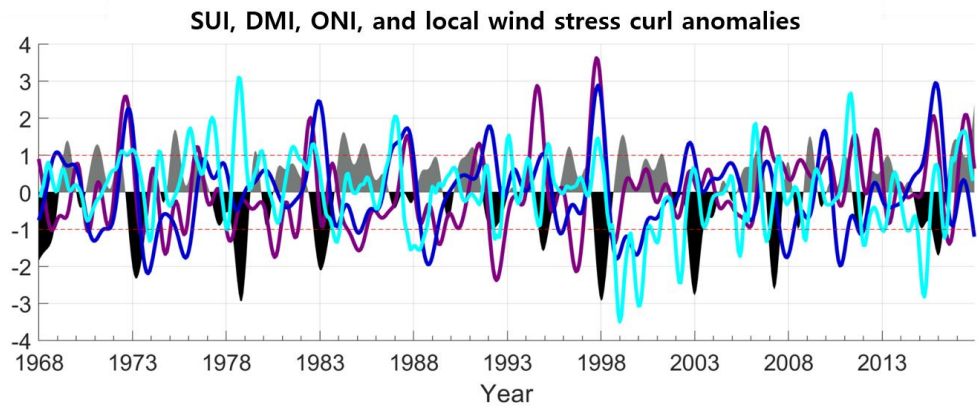

Figure 11. Normalized time series of SUI (shaded black and gray), DMI (purple), ONI (blue), and area-averaged local wind stress curl anomalies in the SCTR (cyan).

References

Chambers, D., B. D. Tapley, and R. H. Stewart. (1999): Anomalous warming in the Indian Ocean coincident with El Niño. *Journal of Geophysical Research*, 104, 3035–3047, doi:10.1029/1998JC900085.

Chakravorty, S., C. Gnanaseelan, J. S. Chowdary, and J.-J. Luo. (2014): Relative role of El Nino and IOD forcing on the southern tropical Indian Ocean Rossby waves. *Journal of Geophysical Research*, 119, 5105-5122, doi: 10.1002/2013JC009713.

Dilmahamod, A. F., J. C. Hermes, and C. J. C. Reason. (2016): Chlorophyll-a variability in the Seychelles-Chagos Thermocline Ridge: Analysis of a coupled biophysical model. *Journal of Marine Systems*, 154, 220-232, doi: 10.1016/j.jmarsys.2015.10.011.

Hermes, J. C. and C. J. C. Reason. (2008): Annual cycle of the South Indian Ocean (Seychelles-Chagos) thermocline ridge in a regional ocean model. *Journal of Geophysical Research*, 113, C04035, doi: 10.1029/2007JC004363.

Jayakumar, A., J. Vialard, M. Lengaigne, C. Gnanaseelan, J. P. McCreary, and B. Praveen Kumar. (2011): Processes controlling the surface temperature signature of the Madden-Julian Oscillation in the thermocline ridge of the Indian Ocean. *Climate Dynamics*, 37, 2217–2234, doi:10.1007/s00382-010-0953-5.

Jury, M. R., B. Pathack, and B. Parker. (1999): Climatic Determinants and Statistical Prediction of Tropical Cyclone Days in the Southwest Indian Ocean. *Journal of Climate*, 12, 1738-1746, doi: 10.1175/1520-0442(1999)012<1738:CDASPO>2.0.CO;2.

Klein, S. A., B. J. Soden, and N.-C. Lau. (1999): Remote sea surface temperature variations during ENSO: Evidence for a tropical atmospheric bridge. *Journal of Climate*, 12, 917–932, doi:10.1175/1520-0442(1999)012<0917:RSSTVD>2.0.CO;2.

Masumoto, Y., and G. Meyers. (1998): Forced Rossby waves in the southern tropical Indian Ocean. *J. Geophys. Res*., 103, 27,589–27,602, doi:10.1029/98JC02546.

McCreary, J. P., P. K. Kundu, and R. L. Molinari. (1993): A numerical investigation of dynamics, thermodynamics and mixed-layer processes in the Indian Ocean. Prog. Oceanogr., 31, 181-224, doi: 10.1016/0079-6611(93)90002-U.

Rao, S. A., and S. K. Behera. (2005): Subsurface influence on SST in the tropical Indian Ocean: Structure and interannual variability. *Dyn. Atmos. Oceans*, 39, 103–135, doi:10.1016/j.dynatmoce.2004.10.014.

Tozuka, T., T. Yokoi, and T. Yamagata. (2010): A modeling study of interannual variations of the Seychelles Dome. *Journal of Geophysical Research*, 115, C04005, doi: 10.1029/2009JC005547.

Ummenhofer, C. C., A. S. Gupta, M. H. England, and C. J. Reason. (2009): Contributions of Indian Ocean Sea Surface Temperatures to Enhanced East African Rainfall. *Journal of Climate*, 22, 993-1012, doi: 10.1175/2008JCLI2493.1.

Vialard, J. P. D., M. J. McPhaden, P. Bouruet-Aubertot, B. Ward, E. Key, D. Bourras, R. Weller, P. Minnett, A. Weill, C. Cassou, L. Eymard, T. Fristedt, C. Basdevant, Y. Dandonneau, O. Duteil, T. Izumo, C. De Boyer Montegut, S.

Masson, F. Marsac, C. Menkes, and S. Kennan. (2009): CIRENE: Air-Sea Interactions in the Seychelles-Chagos Thermocline Ridge Region. *Bulletin of the American Meteorological Society (BAMS)*, 90, 45-61, doi: 10.1175/2008BAMS2499.1

Vinayachandran, P. N., and N. H. Saji. (2008): Mechanisms of south Indian Ocean intraseasonal cooling. *Geophys. Res. Lett*., 35, L23607, doi:10.1029/2008GL035733.

Woodbery, K. E., M. Luther, and J.-J. O'Brien. (1989): The wind-driven seasonal circulation in the southern tropical Indian Ocean. *Journal of Geophysical Research*, 94, 17985-18002, doi: 10.1029/JC094iC12p17985.

Xie, S.-P, H. Annamalai, F. A. Schott, and J. P. McCreary JR. (2002): Structure and Mechanisms of South Indian Ocean Climate Variability. *Journal of Climate*, 15, 864-878, doi: 10.1175/1520-0442(2002)015<0864:SAMOSI>2.0.CO;2.

Yu, W., B. Xiang, L. Liu, and N. Liu. (2005): Understanding the origins of interannual thermocline variations in the tropical Indian Ocean. *Geophysical Research Letter*, 32, L24706, doi: 10.1029/2005GL024327.

Yokoi, T., T. Tozuka, and T. Yamagata. (2008): Seasoanl variation of the Seychelles Dome. *Journal of Climate*, 21, 3740–3754, doi:10.1175/2008JCLI1957.1.

국문 초록

열대 남서인도양 용승 억제 현상 분석

김찬미

지구환경과학부

서울대학교 대학원

열대 인도양 남서부에 위치한 세이셸-차고스 수온약층 언덕(Seychelles-Chagos Thermocline Ridge; SCTR)에서는 남동 무역풍과 적도 편서풍 사이의 음의 바람 응력 회전성에 의해 용승이 발생한다. 이전 연구에 따르면 SCTR 해역의 용승은 동인도양에서 기인하는 원거리 강제력과 연관되어 경년 변동을 보이는 것으로 알려져 있다. 엘니뇨 남방 진동(El Niño-Southern Oscillation; ENSO) 또는 인도양 다이폴(Indian Ocean Dipole; IOD)가 양의 위상을 가질 때 발생하는 동인도양의 동풍 이상치는 하강 로스비파를 서쪽으로 전파시켜 SCTR 해역의 용승을 억제시킨다. 또한 ENSO와 IOD가 동시에 양의 위상을 가진 후에는 SCTR 해역 용승이 더욱 강하게 억제될 수 있다고 알려져 있다. 그러나 최근 연구로부터, SCTR 해역 용승을 억제시키는 요인으로 원거리 강제력 외에도 지역풍의 역할을

무시 할 수 없다는 결과가 발표되었다. 따라서 본 연구에서는 원거리 강제력과 지역풍의 상대적인 중요성을 이해하기 위해 열대 인도양의 장기 재분석장 자료를 1968-2017년 기간 동안 분석하였다. 이 기간 동안 SCTR 해역에서 용승이 억제되었던 9개의 이벤트를 식별한 후, 원거리 강제력과 지역풍의 역할에 초점을 맞추어 각 억제 이벤트의 특성을 연구하였다. 9개의 억제 이벤트들 중 7개는 ENSO와 IOD가 양의 위상을 보인 후에 나타났는데, 알려진 것처럼 동태평양에서 동풍 이상치가 생긴 후 하강 로스비파 이상치가 서쪽으로 전파하여 SCTR 해역의 용승을 억제시킨 것으로 나타났다. 2012년에 용승 억제 피크를 보인 11-12 이벤트는 IOD만 양의 위상을 보인 후에 발생하였는데, ENSO와 IOD가 동시에 양의 위상을 보인 후에 나타났던 7개 이벤트에 비해 하강 로스비파 이상치와 SCTR 해역 용승 억제가 모두 약하게 나타났다. 반면, 78-79 이벤트는 ENSO와 IOD 모두 뚜렷한 양의 위상을 보이지 않은 후에 발생하였는데, 원거리 강제력이 아니라 지역풍에 의해 SCTR 해역을 포함한 그 주변 광범위한 해역까지 용승 억제 현상이 나타났던 것으로 보인다. 본 연구는 기존에 잘 알려졌던 원거리 강제력 뿐만 아니라 지역풍 또한 SCTR 해역의 용승 억제에 기여 할 수 있다는 것을 과거 50년 동안의 자료 분석을 통해 보였으며, 이는 열대인도양 용승 현상의 경년변동성을 이해하고, 나아가 예측하는 데 활용될 수 있을 것으로 생각된다.

주요어: 열대 인도양, 용승, 엘니뇨 남방 진동, 인도양 다이폴, 셰이셸-차고스 수온약층 언덕

학번: 2018-22384